



Systematic Experiments to Determine the Influence of Skew and Rake on Hull Vibratory Excitation Due to Transient Cavitation

J. E. Kerwin, Associate Member, S. D. Lewis, Member
and S. Kobayashi, Visitor, Massachusetts Institute of
Technology, Cambridge, Massachusetts

ABSTRACT

Results of a systematic series of experiments showing the influence of propeller blade skew with and without rake on hull vibratory excitation are presented. These experiments were carried out in a variable pressure water tunnel using a screen generated wake typical of a high-speed single screw cargo ship. These propellers were operated at design advance coefficient and at four cavitation numbers ranging down to a typical value for full speed for this type of vessel. Measurements were made of the vibratory force on a large disc imbedded in a plate above the propeller. These force measurements are intended to be representative, for comparative purposes, of the local propeller vibratory excitation on an actual ship hull. In addition, an extensive series of photographs was obtained for each condition to illustrate the growth and collapse of wake-induced propeller blade cavities.

NOMENCLATURE

A_0 = disc area of propeller, $A_0 = \pi R^2$
 c = section chord length
 C_{TH} = thrust loading coefficient,
 $C_{TH} = T / \frac{1}{2} \rho A_0 V_A^2$
 D = propeller diameter
 f_M = maximum camber of propeller blade section
 K_V = vertical force coefficient on disc,
 $K_V = F_V / \rho n^2 D^4$
 n = propeller revolutions per second
 P = propeller section pitch
 p_∞ = static pressure at depth of propeller hub

p_v = vapor pressure of water
 r = radial distance from propeller axis
 R = propeller radius
 t = maximum thickness of propeller section
 V_A = speed of advance of propeller in open water
 V_s = ship speed
 V_X = local axial flow velocity in ship's wake

$X =$
 $Y =$
 $Z =$
} Cartesian coordinates

β_i = hydrodynamic pitch angle
 θ = angle measured clockwise from z axis when looking upstream
($\theta = 0^\circ$ for vertical downward)
 θ_s = local projected skew angle or warp angle at radius r/R , relative to a radial reference line
 ρ = mass density of water
 $\sigma_n = \frac{p_\infty - p_v}{0.5 \rho n^2 D^2}$
 $\sigma_v = \frac{p_\infty - p_v}{0.5 \rho V_A^2}$

1. INTRODUCTION

As a result of recent research carried out by a number of organizations throughout the world, it is now well established that transient propeller cavitation can be a major source of vibratory excitation of a hull (1). Much effort is now being expended to develop analytical methods of predicting the time history of blade cavitation both with regard to extent and volume, and to determine the exciting forces developed on the hull by this cavitation. Both model and full-scale experiments have been, or are being made to measure these same quantities (1,2,3).

One of these experimental studies

1 Jointly sponsored by the society of Naval Architects and Marine Engineers, Panel H-8, under T&R P.O.#745, and by the U.S. Department of Commerce, Maritime Administration Contract #6-38068.

has been completed at MIT under the sponsorship of SNAME and under the technical administration of Panel H-8, (4). A relatively simple arrangement was devised for the measurement of the propeller-induced vibratory force on a circular disc flush mounted in a flat surface located above the propeller. The measurements showed conclusively that in the extreme wake field used in these tests the cavitation was of principal importance in determining the level of vibratory excitation on the plate. However, this study was limited to one rather extreme wake field, so that the results are not necessarily valid for all ship types.

What is needed, therefore is more extensive data which the designer may use to decide whether or not cavitation-induced vibration is likely to be a major problem. If it is determined that a potential problem exists, the designer is then advised to make use of appropriate experimental and/or analytical techniques for more quantitative information.

A further refinement of the experimental technique developed in (4) was used to generate systematic data on vibratory excitation as a function of cavitation for a series of five 5-bladed propellers operating in a realistic ship wake. These propellers varied systematically from an undistorted parent propeller to similar propellers with 36° and 72° skew respectively and 36° and 72° warp respectively.¹ Cavitation numbers were varied from 6.3 (almost no cavitation) to 1.8, the latter being typical of full speed for the merchant ship. For each propeller, measurements of the first three harmonics of vertical blade frequency vibratory force acting on a disc above the propeller were made.

Since the force measuring disc does not represent an actual hull surface, the test results must be used in a comparative way. In particular, the amount by which the force is altered due to cavitation can serve as a means of correcting vibratory force estimates determined by current non-cavitating methods. The effect of changes in propeller parameters such as skew and warp can be again compared with the corresponding non-cavitating results.

The longitudinal screen generated wake field was measured in the propeller rotational plane, with the propeller removed, using a recently acquired laser-doppler velocimeter. Many measurements were taken in a Y-Z grid, from which the radial distributions of wake harmonics were computed.

For each propeller and for all

four cavitation numbers, a sequence of still pictures was taken at uniform intervals through one blade passage (72°). These photographs show the extent of cavitation at each position, and allow comparison of the effects of cavitation numbers and propeller distortion. These photographic records of transient blade cavitation, together with the corresponding relative vibratory force levels can be used by designers as a means of correlation with specific ship designs and for correlation with theoretical methods.

2. PROCEDURE

2.1 Wake Survey

A longitudinal wake field was generated by a wire screen extending across the test section at a point 53 cm (20.9 in) upstream of the propeller. The wake field generated can be considered typical of a fine-formed single-screw merchant ship with a low average wake fraction and a sharp wake peak.

The measurement of the wake distribution was accomplished using the laboratory's recently acquired Laser-Doppler velocimeter. While the laser system was acquired principally for the measurement of unsteady velocity fields in the neighborhood of an operating propeller, it is well suited for steady velocity measurements.

The test arrangement is illustrated in Figure 1. The transmitting and receiving optics of the laser system are located on a common base which can be moved vertically and horizontally.

¹ An undistorted propeller has the blade section mid chord points lying along straight radial lines in the rotational plane.

A skewed propeller has the blade section mid-chord points lying along a fair curve on the pitch helix. The skew angle at the propeller tip is defined in the rotational plane as the angle between a radial line from the centerline of the propeller hub through the mid-chord point of the propeller root sections and a radial line from the center of rotation through the projection of the propeller tip on the rotational plane.

A warped propeller has the blade section mid-chord points lying along a fair curve in the plane of rotation. The warp angle at the propeller tip is defined as the angle in the plane of rotation between a radial line from the centerline of the propeller hub through the mid-chord point of the propeller root section and a radial line from the center of rotation through the propeller tip.

The wake field can therefore be measured most conveniently in a Cartesian grid in the plane of the propeller. A finer grid spacing was used in the high wake region when higher resolution was required. The output of the signal processor is a voltage, directly proportional to velocity, which can be averaged electronically to provide accurate measurements at each grid point.

A disadvantage of the Cartesian grid is that measurements must be converted to cylindrical coordinates to enable the usual harmonic analysis of the wake field to be performed. We had considered moving the laser base in constant increments of radius and rotation angle, but had concluded that there would be less freedom of motion if only one degree of freedom was required. Obviously a fully automated positioning system for the laser base would be ideal for this purpose.

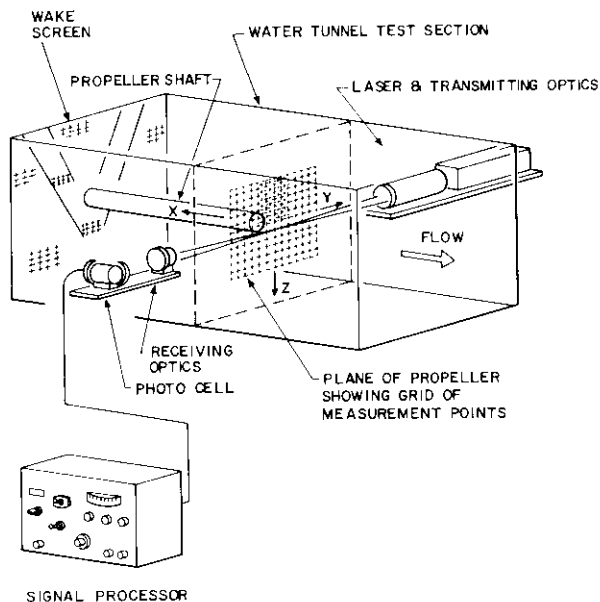


Fig. 1 Experimental Setup for Wake Survey

2.2 Force Measurements

2.2.1 Hull Simulation and Force Measurement Disc. The test arrangement is illustrated in Figure 2. An extremely rigid simulated hull is constructed of solid aluminum, and is attached to the upper window of the test section. The depth of the hull is designed to provide a tip clearance of 20% of the 304.8 mm (12 in) propeller diameter. The bottom of the hull is flat except at the leading and trailing edges where streamlining was provided.

An exploded view of the force

measuring device is shown in Figure 3a, and a sectional view of the device is shown in Figure 3b. The force measurement disc is an aluminum plate 180 mm (7 in) in diameter with a thickness of 13 mm (0.5 in), mounted flush with the hull surface. Water is excluded from the cavity above the disc by an "O" ring seal. The disc is connected to a 136 Kg (300 lb) strain-gage load cell which, in turn, is connected to an extremely heavy aluminum dome.

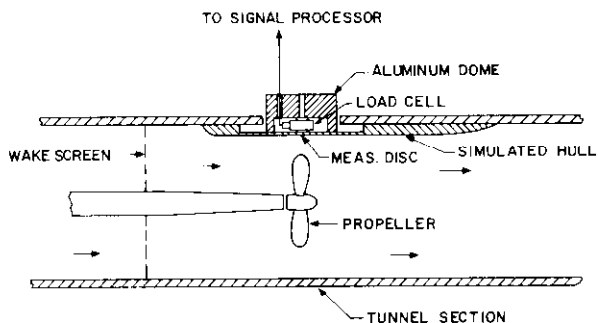


Fig. 2 Test Section Arrangement

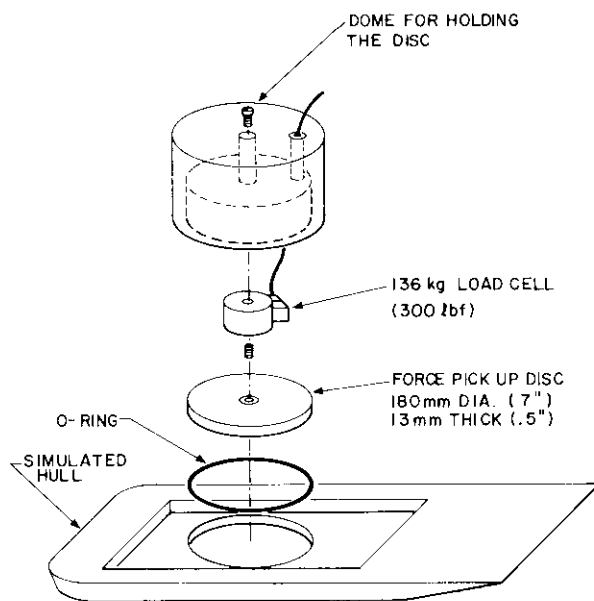


Fig. 3a. Force Measuring Device - Exploded View

The air space inside the cavity is sealed from the atmosphere as well as from the tunnel, and its pressure may be altered by means of the tunnel's vacuum system. This was found to be necessary for two practical reasons. At low cavitation numbers, the differential pressure on the disc would overload the strain-gage load cell unless the cavity pressure was correspondingly reduced. On the other hand, a small positive differential between the cavity pressure and test section static pressure was essential to prevent water from leaking

into the cavity and damaging the load cell. This arrangement proved to be very reliable and simple to use.

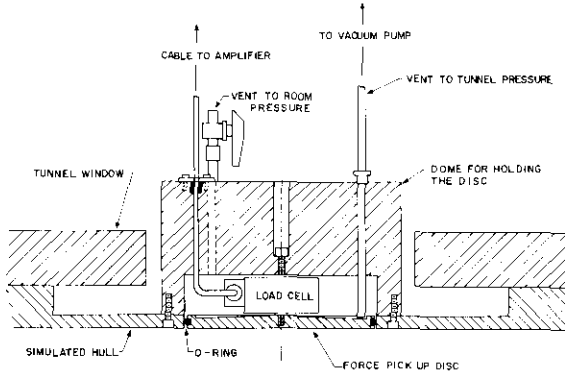


Fig. 3b Force Measuring Device - Sectional View

While the position of the disc is fixed, the propeller drive can be moved longitudinally. During the force tests, measurements were made with the propeller tips directly below the upstream edge, center, and downstream edge of the disc as shown in Figure 4. This corresponds to a longitudinal travel of $\pm 59\%$ of the propeller radius.

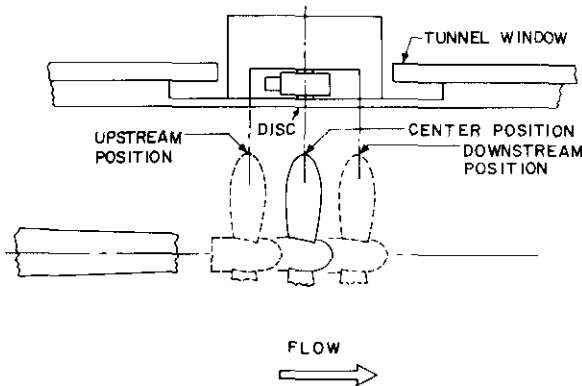


Fig. 4 Force Test Propeller Locations

2.2.2 Measurement System and Calibration. A block diagram of the measurement system is shown in Figure 5. The load cell is connected to a carrier type strain-gage amplifier which provides a direct readout of the steady load, and provides an amplified, demodulated unsteady force output. The steady readout is used both for static calibration and for monitoring of the pressure differential between the tunnel and the dome.

The amplifier output is processed by a waveform eductor which is triggered at blade frequency by a magnetic pick-up on the propeller shaft. The eductor averages repeated values of the signal

following any specified number of blade frequency trigger pulses. The averaged signal retains all harmonics of blade frequency while greatly attenuating periodic components not related to blade frequency and random components due to turbulence, cavity bubble dynamics and extraneous noise. While some of the latter may actually be present in the full-scale flow, previous experimental records processed by a spectrum analyzer indicated that the discrete peaks at multiples of blade frequency stood well above the broad band component of the spectrum. This is no doubt fortunate since the proper interpretation of the latter with regard to scaling would be most difficult.

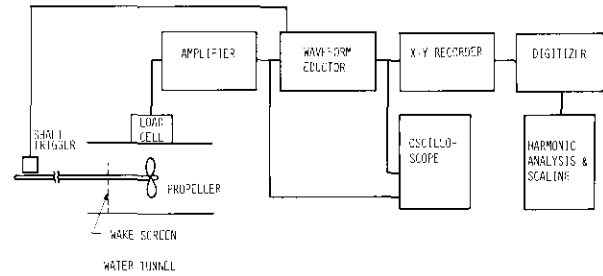


Fig. 5 Block Diagram of Measurement System

The final averaged signal may be viewed on an oscilloscope or plotted on an x-y pen recorder. At the time of the present experiments there was no direct means of transmitting the averaged signal to a digital computer for the final step of scaling and harmonic analysis. As an interim measure, this step was accomplished by taking the graphs to a mini-computer equipped with a digitizer, and tracing the records by hand.

The capacity of the load cell was selected on the basis of the usual compromise between sensitivity and natural frequency. It was determined that the processing system signal to noise ratio would be adequate if the average force amplitude was as low as five percent of the nominal capacity of the load cell. This would then result in a natural frequency in the neighborhood of 5 times blade frequency, thus permitting accurate estimate of force components up to three times blade frequency. A higher capacity load cell would result in a higher natural frequency but would reduce the signal levels to a point where the signal/noise ratio would be too low.

A static calibration of the system was readily done with known weights and the output of the strain-gage amplifier. Dynamic calibration was achieved by

means of an electromagnetic shaker and impedance head.

A dynamic calibration was first done in air, with and without the O-ring seal, and the results are shown in Figure 6.

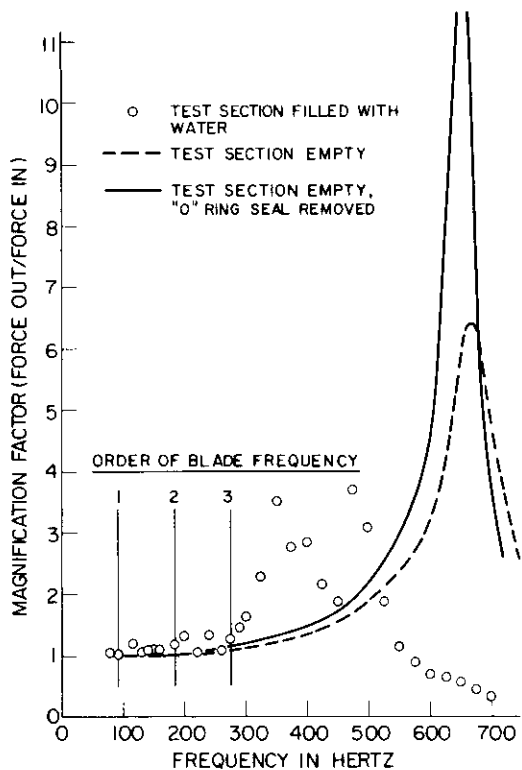


Fig. 6 Dynamic Calibration of Measuring System

The natural frequency is approximately 660 Hz, which is close to the value anticipated on the basis of a simple one degree of freedom model. The additional damping provided by the O-ring greatly reduces the resonance peak, and has a negligible effect elsewhere.

For a planned test speed of 1100 RPM, blade frequency corresponds to 91.67 Hz for a five bladed propeller, and it is evident that the response curve in air is nearly flat to well beyond three times blade rate.

An estimate of the change in natural frequency due to the added mass of the disc with water in the test section indicated that the response would still be satisfactory for measurement up to three times blade frequency. The equipment was therefore installed in the tunnel, and a dynamic calibration performed in water. In this case, a connecting shaft had to be located between the impedance head and the disc, since the former could not be located under water. The shaft was made as light as possible, and the influence of its mass was accounted for in the calibration.

The final dynamic calibration in water is also shown in Figure 6. There now appears to be a double resonance, which may possibly be due to a resonance of the connecting shaft. If this is the case, its effect would not be present in the actual experiments.

Fortunately the behaviour at resonance is of no practical concern, and the final calibration shows a nearly flat response up to three times blade frequency. It is also clear that no attempt should be made to extract any data for higher frequencies from the measured signals. Figure 7 shows a sample of the averaged signal for one propeller longitudinal position, together with the reconstructed signal using the first three harmonics of blade frequency.

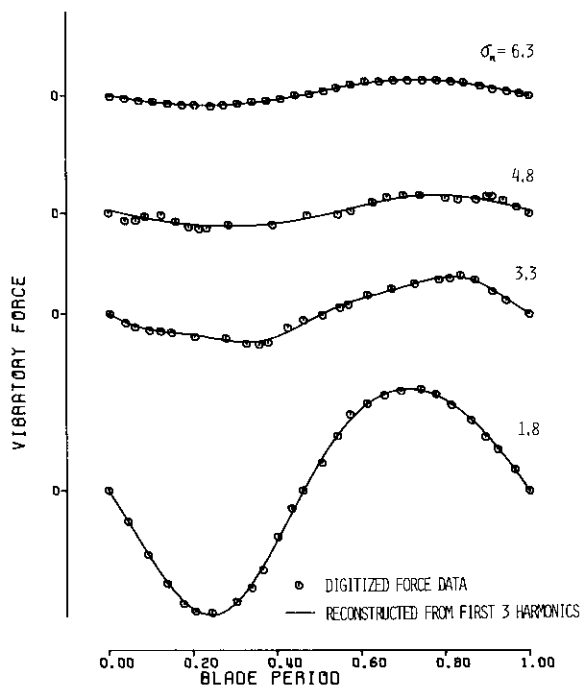


Fig. 7 Sample of the Digitized Force Data Together with the Reconstructed Signal Using the First Three Harmonics of Blade Frequency

2.2.3 Experiments A systematic series of measurements were made using a set of five propellers designed by DTNSRDC with varying skew and warp (5,6,7). The characteristics of the propeller series are given in Table I and the propeller designation in Table II. These propellers all have the same radial distribution of chord length and thickness, and were designed to have the same loading distribution at an advance coefficient of $J=0.889$. The series is therefore ideal in making possible the investigation of the importance of large changes in skew and warp without extraneous influences.

TABLE I

Geometry of Propellers

(Reproduced from (5,6,7))

Number of Blades	5
Expanded Area Ratio	0.725
Section Meanline	NACA a=0.8
Section Thickness Distribution	NACA 66 with NRSDC modified nose and tail
Design J	0.889
Design C _{TH}	0.686

r/R	tanβ _i	c/D	t/c
0.2	1.8256	0.174	0.2494
0.3	1.3094	0.229	0.1562
0.4	1.0075	0.275	0.1068
0.5	0.8034	0.312	0.0768
0.6	0.6483	0.337	0.0566
0.7	0.5300	0.347	0.0421
0.8	0.4390	0.334	0.0314
0.9	0.3681	0.280	0.0239

Propeller 4381 (Skew =0 Deg)

r/R	θ _s (deg)	P/D	f _M /c
0.3	0.0	1.3448	0.0368
0.4	0.0	1.3580	0.0348
0.5	0.0	1.3361	0.0307
0.6	0.0	1.2797	0.0245
0.7	0.0	1.2099	0.0191
0.8	0.0	1.1366	0.0148
0.9	0.0	1.0660	0.0123

Propeller 4382 (Skew =36 Deg)

r/R	θ _s (deg)	P/D	f _M /c
0.3	4.655	1.4432	0.0370
0.4	9.363	1.4117	0.0344
0.5	13.948	1.3613	0.0305
0.6	18.378	1.2854	0.0247
0.7	22.747	1.1999	0.0199
0.8	27.145	1.1117	0.0161
0.9	31.575	1.0270	0.0134

Propeller 4383 (Skew =72 Deg)

r/R	θ _s (deg)	P/D	f _M /c
0.3	9.293	1.5124	0.0407
0.4	18.816	1.4588	0.0385
0.5	27.991	1.3860	0.0342
0.6	36.770	1.2958	0.0281
0.7	45.453	1.1976	0.0230
0.8	54.245	1.0959	0.0189
0.9	63.102	0.9955	0.0159

Propeller 4497 (Warp =36 Deg)

r/R	θ _s (deg)	P/D	f _M /c
0.3	4.655	1.4332	0.0370
0.4	9.363	1.4117	0.0344
0.5	13.948	1.3613	0.0305
0.6	18.378	1.2854	0.0247
0.7	22.747	1.1999	0.0199
0.8	27.145	1.1117	0.0161
0.9	31.575	1.0270	0.0134

Propeller 4498 (Warp =72 Deg)

r/R	θ _s (deg)	P/D	f _M /c
0.3	9.293	1.5124	0.0407
0.4	18.816	1.4588	0.0385
0.5	27.991	1.3860	0.0342
0.6	36.770	1.2958	0.0281
0.7	45.453	1.1976	0.0230
0.8	54.245	1.0959	0.0189
0.9	63.102	0.9955	0.0159

TABLE II
Propeller Designation

Propeller Model Number	Geometric Characteristics	Present Designation
4381	0° Skew	0S
4382	36° Skew	36S
4383	72° Skew	72S
4497	36° Warp	36W
4498	72° Warp	72W

All experiments were run at the design advance coefficient and with four values of the cavitation number. Since the experiments are not intended to represent any particular ship, one cannot translate cavitation number precisely to speed. However, if we assume a tip submergence of 3 meters, (9.84 ft), and a wake fraction of 0.22, a ship speed of 26 knots corresponds to a cavitation number of

$$\sigma_n = \frac{p_\infty - p_v}{\frac{1}{2} \rho n^2 D^2} = 1.8$$

which would be reasonable top speed for a ship with this type of wake field.

With the tunnel operating at atmospheric pressure at 1100 propeller revolutions per minute, the resulting cavitation number is $\sigma_n = 6.3$. Dividing this interval of cavitation numbers evenly, we obtain the following four test conditions,

Condi- tion	$\sigma_n = \frac{P_\infty - P_V}{\frac{1}{2} \rho n^2 D^2}$	$\sigma_V = \frac{P_\infty - P_V}{\frac{1}{2} \rho V_A^2}$	Representative V_s (Knots)
1	6.3	8.0	14
2	4.8	6.1	16
3	3.3	4.2	19.5
4	1.8	2.3	26

2.3 Photography of Transient Cavitation

The total time for a complete cycle of cavity growth is of the order of 1/50 second, so that the phenomenon can only be studied by means of high-speed photography. Motion pictures taken at 7500 frames per second and above are feasible, but require elaborate lighting procedures and the small negative size limits the quality of prints made of individual frames (8).

If the flow phenomenon is truly periodic, a sequence of individual still photographs taken with uniform intervals of time delay relative to the position of a blade should produce the same result. Obviously the phenomenon is not entirely repeatable, so that the details of the flow as seen in successive photographs will not necessarily appear consistent, since one is not looking at one cycle of the same event. For the present experiments, the repeatability of each cycle is remarkable, and one could easily mistake a timed sequence of stills for a print of a short segment of a high speed movie.

The photographic sequences which are presented were obtained by a succession of precisely controlled time delays selected to produce an angular increment of four degrees of propeller rotation angle. A total of eighteen photographs therefore covers one blade period and one cavitation number for a five-bladed propeller.

The best viewing location for pictures is from above because the most severe wake in this case is near top center, and from upstream as the cavitation of interest is on the back (upstream side) of the blade. This required a modification to the test section configuration. Fortunately, by removing the instrumented disc, it was possible to install a viewing port inclined upstream at 30 degrees to the vertical which obtained an adequate view of the cavitation phenomena. A sketch of the test section arrangement for photography appears in Figure 8. The viewing port is constructed of clear acrylic and filled with water in order to reduce distortion due to refraction at the window.

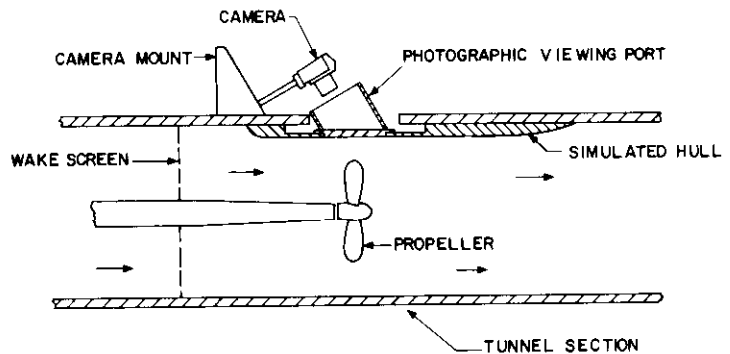


Fig. 8 Test Section Arrangement for Photography

A 35 mm single lens reflex camera with a wide-angle lens provided the necessary field of view through the port. A strobe light was positioned on either side of the test section to light the propeller without shadows. Since depth of focus was critical it was found necessary to stop down the lens to f16. At this lens setting, it was necessary to use high speed film (TRI-X) and extra development time (one stop) to achieve adequate film density.

3. RESULTS

3.1 Wake Harmonics

To obtain the harmonics of the wake, it was assumed that the velocity could be expressed in the form

$$\frac{v_x(r, \theta)}{V_s} = \sum_{m=0}^4 \{ a_{0m} + \sum_{n=1}^{10} a_{nm} \cos n\theta + \sum_{n=1}^{10} b_{nm} \sin n\theta \} \left(\frac{r}{R}\right)^m \quad (1)$$

where a_{nm} and b_{nm} constitute a total of 105 unknown coefficients to be determined. These can be obtained by solving the set of simultaneous equations generated from (1) by substituting the value of r and θ and the resulting measurement of V_x at each of the grid points. In principle, measurement at 105 grid points would permit the determination of the unknown coefficients. However, it is generally advisable to have a larger number of measurement points, and to solve the resulting system of equations by least squares. In this case 223 measurement points were used and coefficients a_{nm} , b_{nm} were calculated. Furthermore, using these coefficients, we can write the velocity in the form of a finite Fourier series with respect to θ , for given values of r ; for example, $r/R = .3, .4, \dots, 1.0$. Eq. (1) is rewritten

$$\frac{V_x(r, \theta)}{V_s} = \sum_{m=0}^4 a_{0m} \left(\frac{r}{R}\right)^m + \sum_{n=1}^{10} \left[\sum_{m=0}^4 a_{nm} \left(\frac{r}{R}\right)^m \right] \cos n\theta + \left[\sum_{m=0}^4 b_{nm} \left(\frac{r}{R}\right)^m \right] \sin n\theta \quad (2)$$

$$\equiv A_0 + \sum_{n=1}^{10} [A_n \cos n\theta + B_n \sin n\theta] \quad (3)$$

where

$$A_0 = \sum_{m=0}^4 a_{0m} \left(\frac{r}{R}\right)^m$$

$$A_n = \sum_{m=0}^4 a_{nm} \left(\frac{r}{R}\right)^m$$

$$B_n = \sum_{m=0}^4 b_{nm} \left(\frac{r}{R}\right)^m$$

The resulting values of coefficients are given in Table III.

The resulting wake field distribution is plotted in Figure 9.

TABLE III
Harmonics of Screen Wake
Longitudinal Component

N	0.300R		0.400R	
	A(N)	B(N)	A(N)	B(N)
0	0.8428	0.0000	0.9346	0.0000
1	0.0843	0.1123	0.1200	0.0439
2	-0.1144	0.0808	-0.1623	0.0479
3	0.0199	-0.0045	0.0496	0.0084
4	0.0046	-0.0230	0.0176	-0.0282
5	-0.0339	-0.0261	-0.0207	-0.0102
6	-0.0001	-0.0126	0.0022	-0.0157
7	0.0159	-0.0530	-0.0026	-0.0385
8	-0.0508	-0.0977	-0.0001	-0.0583
9	-0.1256	-0.0407	-0.0763	-0.0248
10	-0.0886	0.0476	-0.0512	0.0231

N	0.500R		0.600R	
	A(N)	B(N)	A(N)	B(N)
0	0.9807	0.0000	0.9957	0.0000
1	0.1502	-0.0010	0.1707	-0.0207
2	-0.1796	0.0196	-0.1766	-0.0021
3	0.0674	0.0193	0.0782	0.0229
4	0.0109	-0.0281	0.0088	-0.0226
5	-0.0134	-0.0042	-0.0104	-0.0029
6	0.0052	-0.0105	0.0068	-0.0032
7	-0.0096	-0.0264	-0.0088	-0.0155
8	0.0189	-0.0278	0.0167	-0.0063
9	-0.0345	-0.0124	-0.0039	-0.0053
10	-0.0233	0.0007	-0.0055	-0.0152

N	0.700R		0.800R	
	A(N)	B(N)	A(N)	B(N)
0	0.9963	0.0000	1.0010	0.0000
1	0.1788	-0.0129	0.1733	0.0255
2	-0.1669	-0.0174	-0.1675	-0.0287
3	0.0865	0.0142	0.0971	-0.0107
4	-0.0310	-0.0115	-0.0411	0.0047
5	-0.0112	-0.0010	-0.0161	0.0064
6	0.0050	0.0011	-0.0025	-0.0022
7	-0.0031	-0.0059	0.0050	0.0011
8	0.0042	0.0068	-0.0076	0.0125
9	0.0136	-0.0036	0.0176	-0.0053
10	0.0028	-0.0226	0.0035	-0.0212

N	0.900R		1.000R	
	A(N)	B(N)	A(N)	B(N)
0	1.0306	0.0000	1.1077	0.0000
1	0.1542	0.0983	0.1229	0.2101
2	-0.1989	-0.0410	-0.2851	-0.0615
3	0.1147	-0.0550	0.1440	-0.1214
4	-0.0207	0.0257	0.0529	0.0508
5	-0.0261	0.0239	-0.0432	0.0559
6	-0.0177	-0.0172	-0.0432	-0.0471
7	0.0139	0.0032	0.0226	-0.0036
8	-0.0073	0.0122	0.0163	0.0082
9	0.0093	-0.0069	-0.0082	-0.0028
10	-0.0002	-0.0130	-0.0040	-0.0019

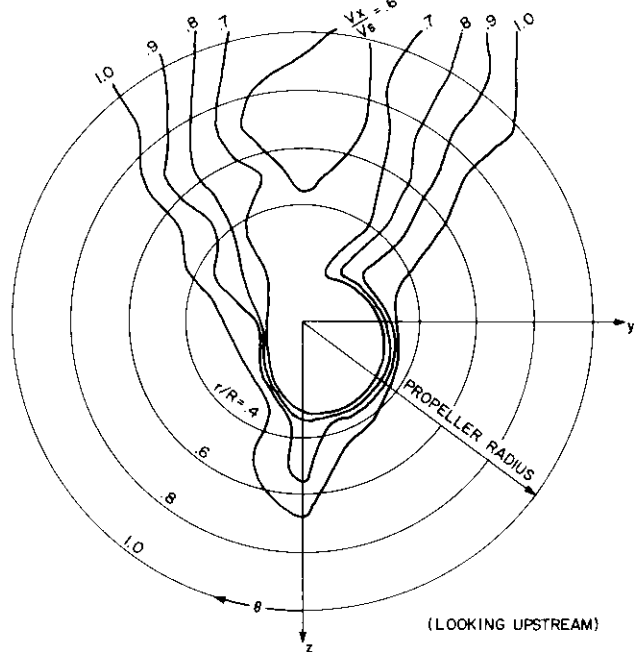


Fig. 9 Measured Wake Field

3.2 Results of Force Measurements

The amplitudes of the blade frequency harmonic of the vibratory force on the disc as a function of cavitation number are given in Figures 10-12 for all five propellers of the series at the 3 longitudinal locations. The vibratory force is expressed both as a percent of the time-average propeller thrust and as a force coefficient

$$K_V = \frac{F_V}{\rho n^2 D^4}$$

based on propeller rotational speed and diameter. Since both propeller thrust and speed of rotation were held constant during the experiments, these two forms of nondimensionalization differ by a constant scale factor and therefore are represented by two scales on the same graph.

The amount of cavitation present at the highest cavitation number was negligible, except for a steady hub vortex, so that these results can be interpreted as the non-cavitating limit. There is a clear correlation between vibratory force amplitude and skew. A skew of 36° reduces the force to 60% of the value for no skew, while 72° skew reduces the force to around 20%. The latter force is so small that precise measurement is extremely difficult!

In the non-cavitating condition, the warped propellers behave in exactly the same way as the skewed propellers. Elimination of skew induced rake, if desirable for other considerations, is therefore not to be discouraged from the point of view of non-cavitating vibratory force. There is also a trend to lower vibratory force as the propeller is moved successively to the downstream (Figure 11) and then the upstream (Figure 12) test location.

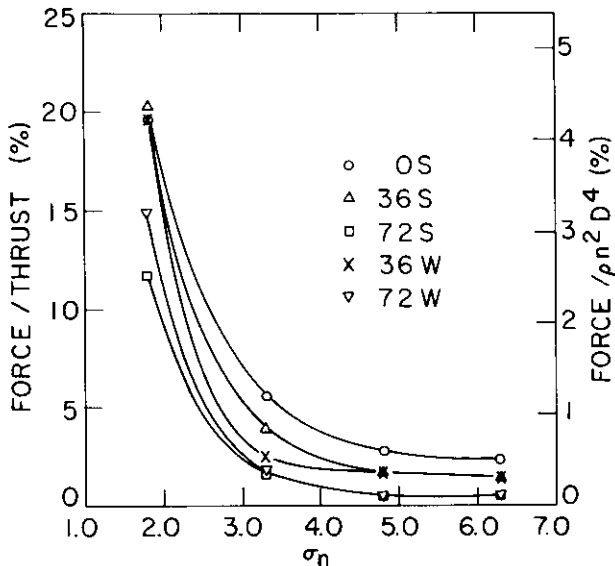


Fig. 10 Blade Frequency Harmonic of Force Data for Five Propellers with Propeller Tip Under Disc Center

As the cavitation number is decreased, the vibratory force increases slowly at first and then almost exponentially for all the propellers as σ_n approaches 1.8. Earlier experiments (4) have shown that vibratory force reaches a peak somewhere below

$\sigma_n=2.0$ and then declines abruptly as cavitation number approaches zero. With the data available we cannot determine the relationship of values given at $\sigma_n=1.8$ to the peak vibratory force. The data does show that the undistorted propeller generally produces substantially more vibratory force than any of the other propellers tested. The 36° skew and the 36° warp propellers produce less vibratory force than the undistorted propeller at all cavitation numbers down to $\sigma_n=3.3$, with the 36° warp propeller slightly better than the 36° skew propeller. At $\sigma_n=1.8$ the trend is less obvious, possibly due to scatter in the data. Nevertheless, on an average these propellers are still superior to the undistorted propeller. The trend continues to the 72° skew and 72° warp propellers which produce substantially less vibratory force than the previous propellers in all cases, once again allowing for some scatter. Only at the lowest cavitation number the 72° skew propeller is shown to be superior to the 72° warp propeller in reducing vibratory force due to cavitation.

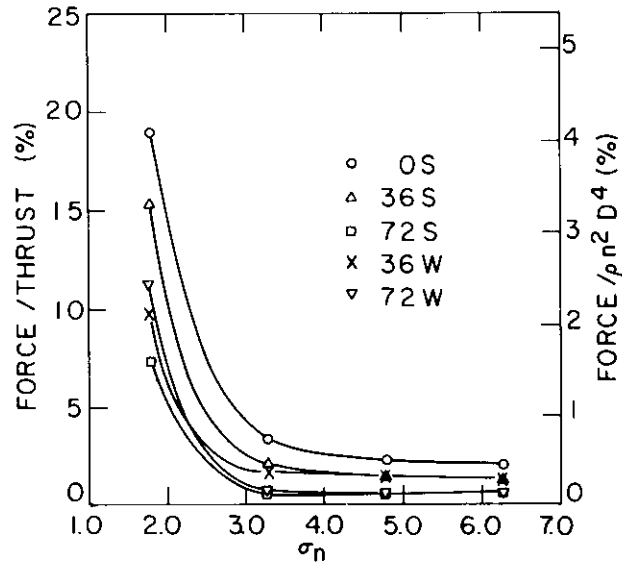


Fig. 11 Blade Frequency Harmonic of Force Data for Five Propellers With Propeller Tip Moved Down-Stream 0.59R

The phase angles of the measured force at blade frequency harmonic are essentially independent of longitudinal position, so that one can therefore expect that the total force acting on a hull surface would be greater than the values measured on the disc.

Figures 13-15 show the vibratory force amplitudes of the first 3 harmonics of blade frequency for the 0° skew propeller, at the three tested longitudinal positions.

Contrary to our expectations (2,9), the amplitudes of the second and third

harmonics are substantially lower than the blade frequency component in all cases. Some of the raw signals gave the appearance of larger higher harmonics, but these proved to be largely fourth and fifth harmonics of blade frequency which were being amplified by the system resonance and which could therefore not be measured with confidence. On the other hand, we are reasonably confident of the second and third harmonics in view of the extensive dynamic calibration of the system,

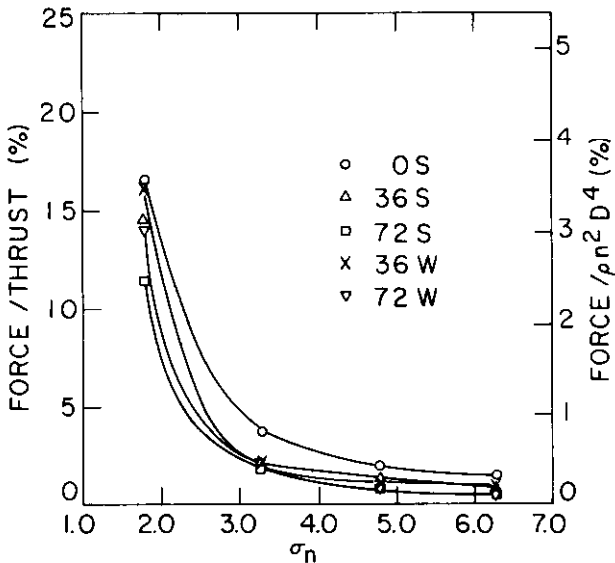


Fig. 12 Blade Frequency Harmonic of Force Data for Five Propellers with Propeller Tip Moved Upstream 0.59R

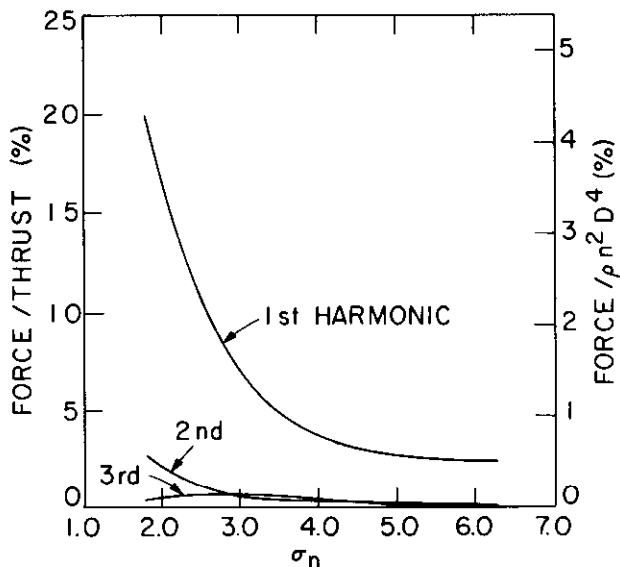


Fig. 13 Three Harmonics of Force Data for Propeller 0S with Propeller Tip Under Disc Center

One possible reason is that there is a phase shift in the pressure signals of 2nd and 3rd harmonics, which depends on the relative location between

the source of pressure and the transducer. Since the force pick up disc has a finite area, these pressure signals may cancel each other on the disc. This fact has been implied by another experiment which is now going on at the water tunnel of Marine Hydrodynamics Laboratory, M.I.T.

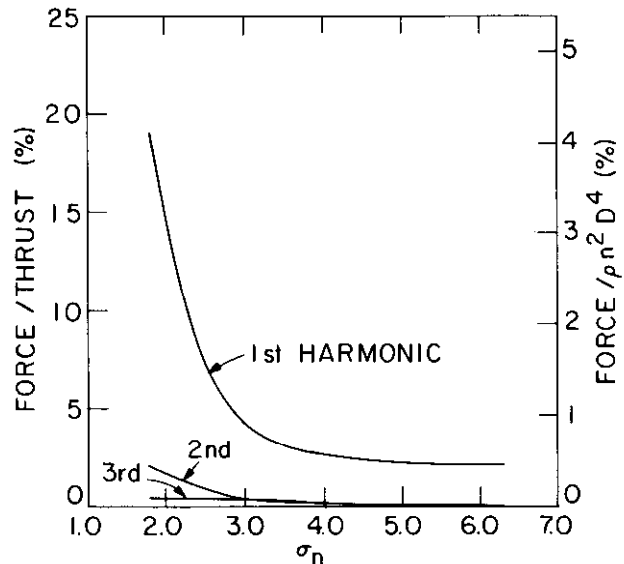


Fig. 14 Three Harmonics of Force Data for Propellers 0S with Propeller Tip Moved Downstream 0.59R

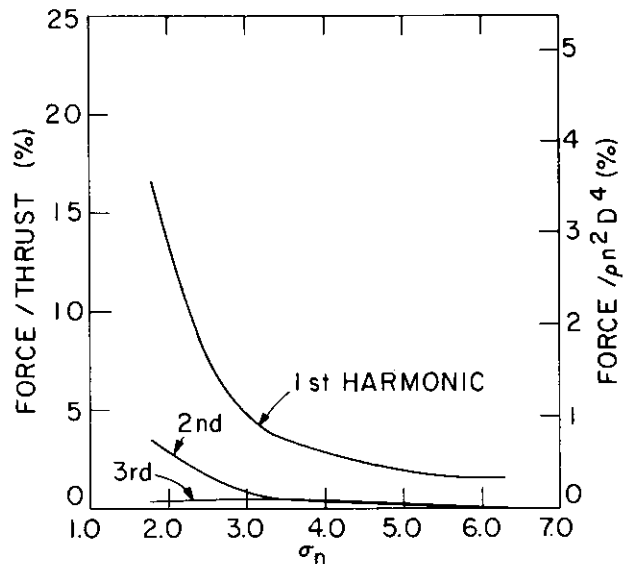


Fig. 15 Three Harmonics of Force Data for Propeller 0S with Propeller Tip Moved Upstream 0.59R

The longitudinal distribution of force has a peak at the propeller tip for the first harmonic. On the other hand, for the 2nd harmonic, the shape of the distribution is such that the higher value shows up as the propeller is moved downstream. This might suggest that the source of second harmonic component lies in the tip vortex cavitation apart from the blade. The first harmonic, on the contrary, seems to come out from the blade

attached cavitation. This difference of source may explain the fact that the second harmonic has phase shift whereas the first does not.

Figures 16-19 show the same results for the remaining propellers of the series. Only the central longitudinal propeller position is given, since the other results show identical trends. The higher harmonics are still small, but do not decrease with skew and warp to the extent that the fundamental does. Their relative influence is therefore somewhat greater as skew is increased.

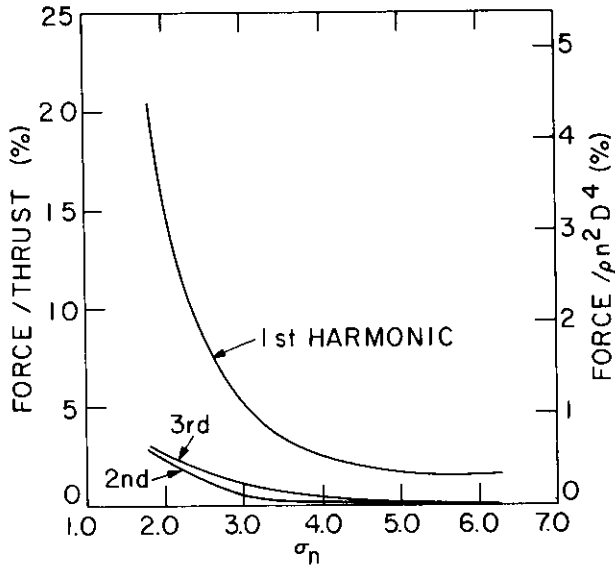


Fig. 16 Three Harmonics of Force Data for Propeller 36S with Propeller Tip Under Disc Center

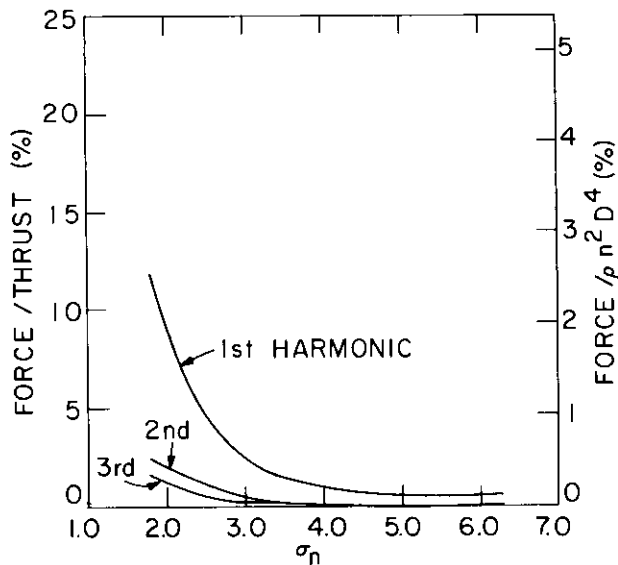


Fig. 17 Three Harmonics of Force Data for Propeller 72S with Propeller Tip Under Disc Center

The wall effect of the water tunnel test section on vibratory force has not been evaluated in such a manner

as indicated in reference (10). A precise investigation of this effect should be done. However, it is felt that the comparative results which have been obtained are useful and accurate, particularly since all tests were run at the same propeller frequency (RPM).

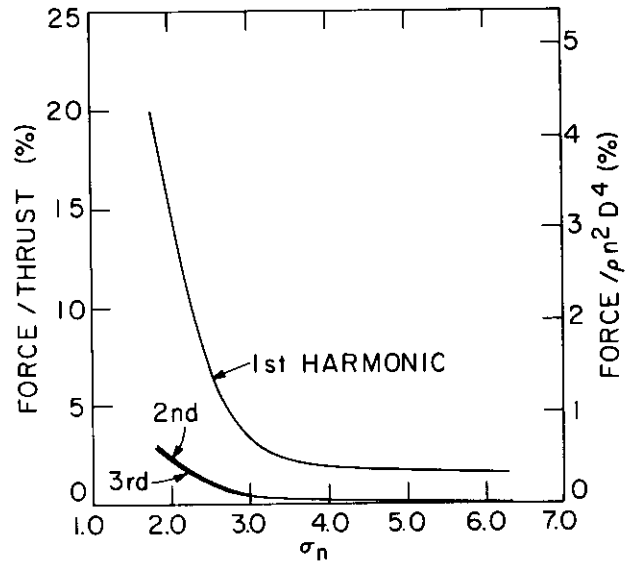


Fig. 18 Three Harmonics of Force Data for Propeller 36W with Propeller Tip Under Disc Center

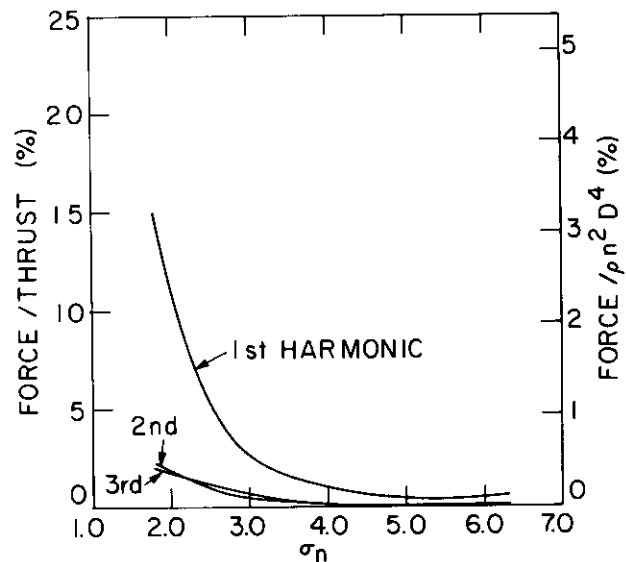


Fig. 19 Three Harmonics of Force Data for Propeller 72W with Propeller Tip Under Disc Center

Other calibration tests of the water tunnel circuit were made previously. A sinusoidal volume variation was introduced at the test section wall and the resulting response was also measured in the test section (11). No resonance was measured in the frequency range of these tests.

3.3 Photographs of Cavitation

The photographs reveal both the max-

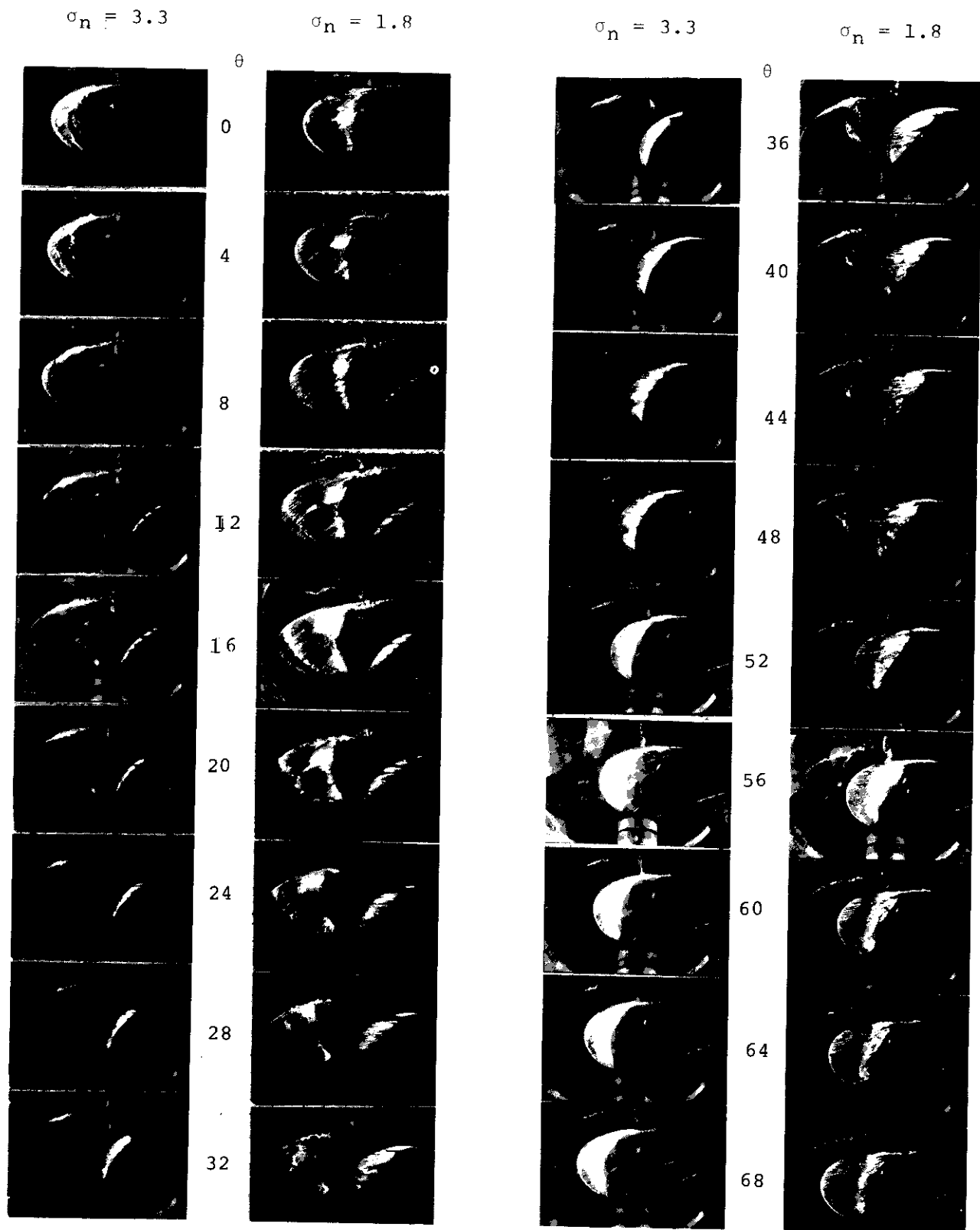


Fig. 20 Propeller OS pictured at Intervals of 4° and at Two Values of σ_n

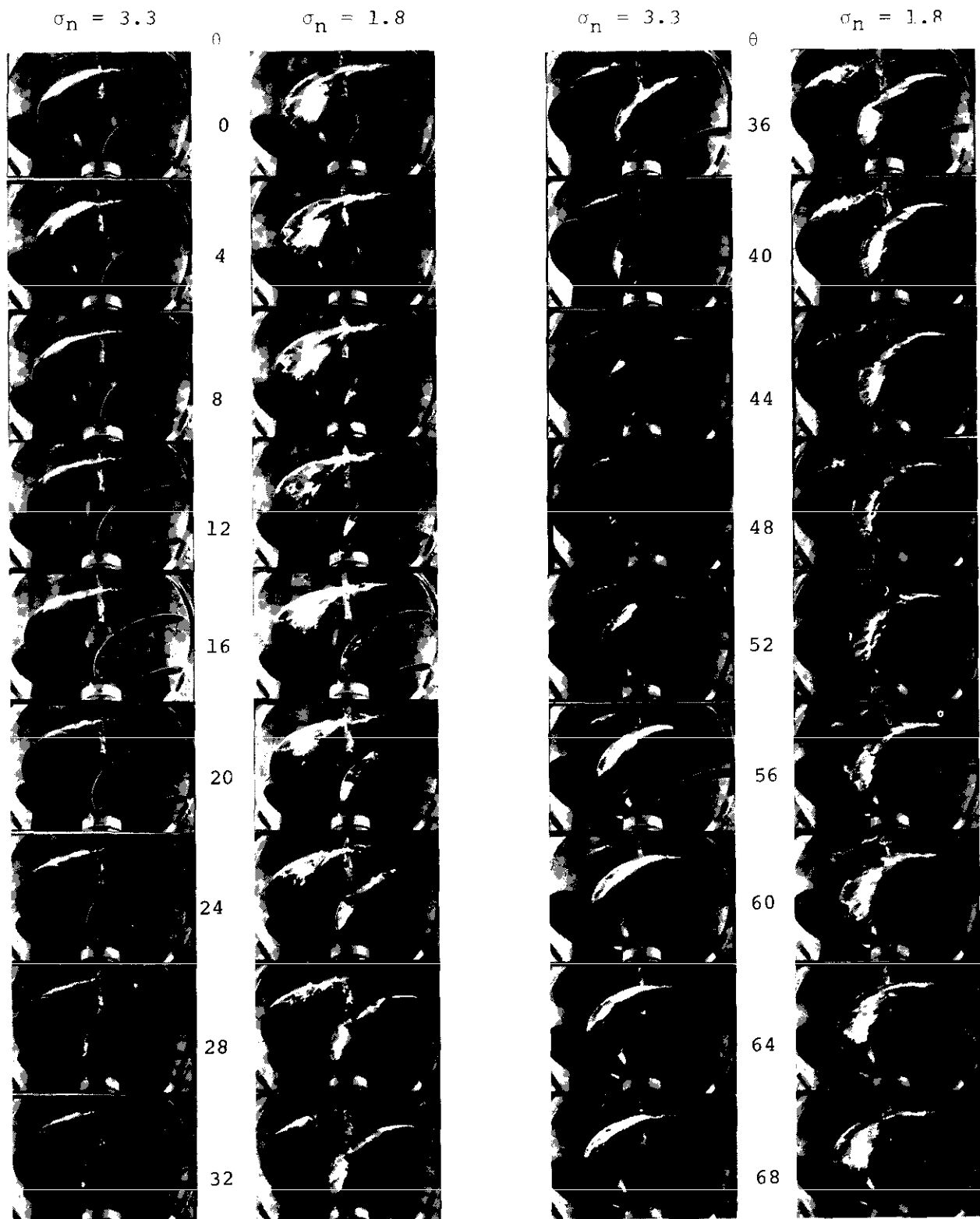


Fig. 21 Propeller 36S Pictured at Intervals of 4° and at Two Values of σ_n

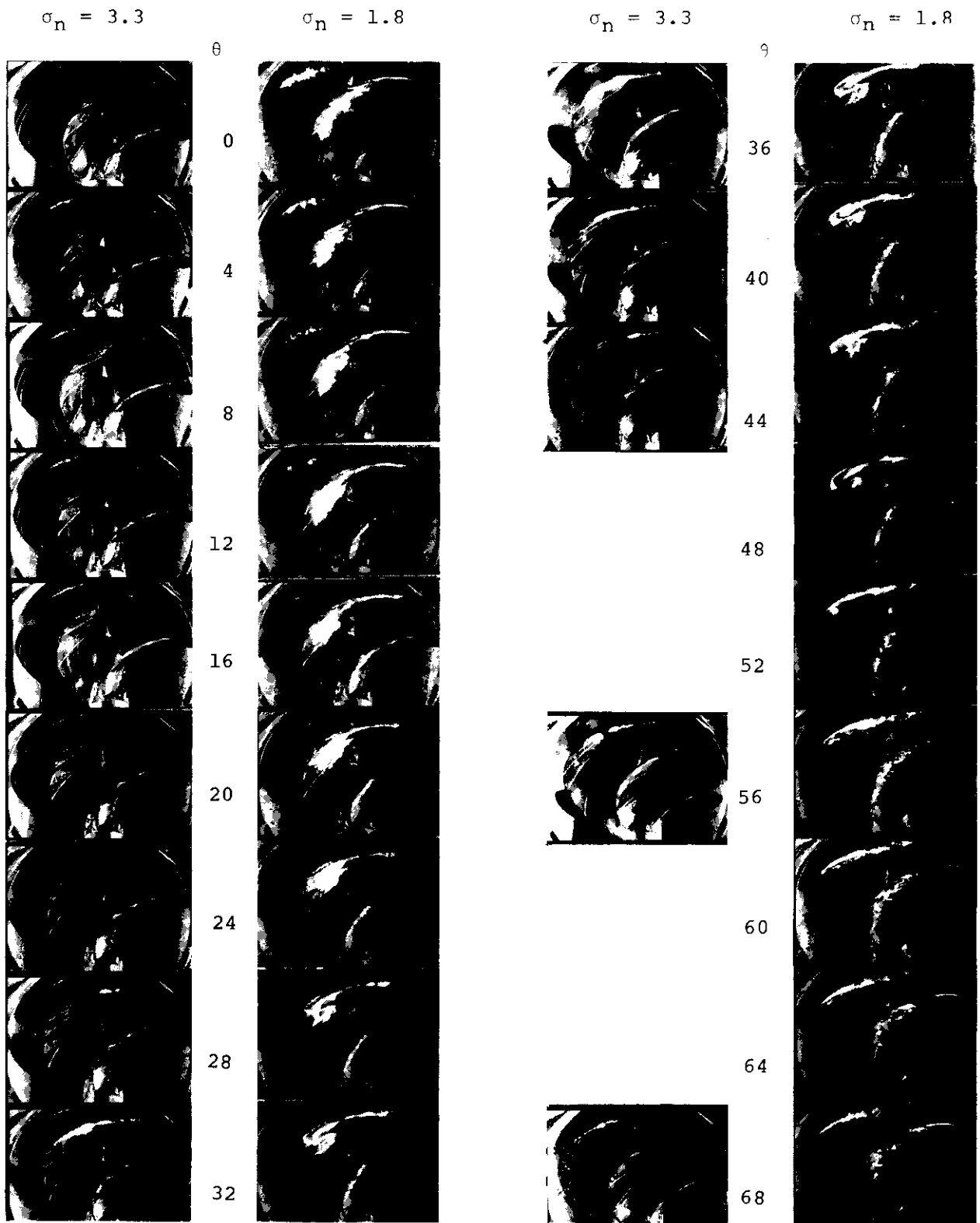


Fig. 22 Propeller 72S Pictured at Intervals of 4° and at Two Values of σ_n

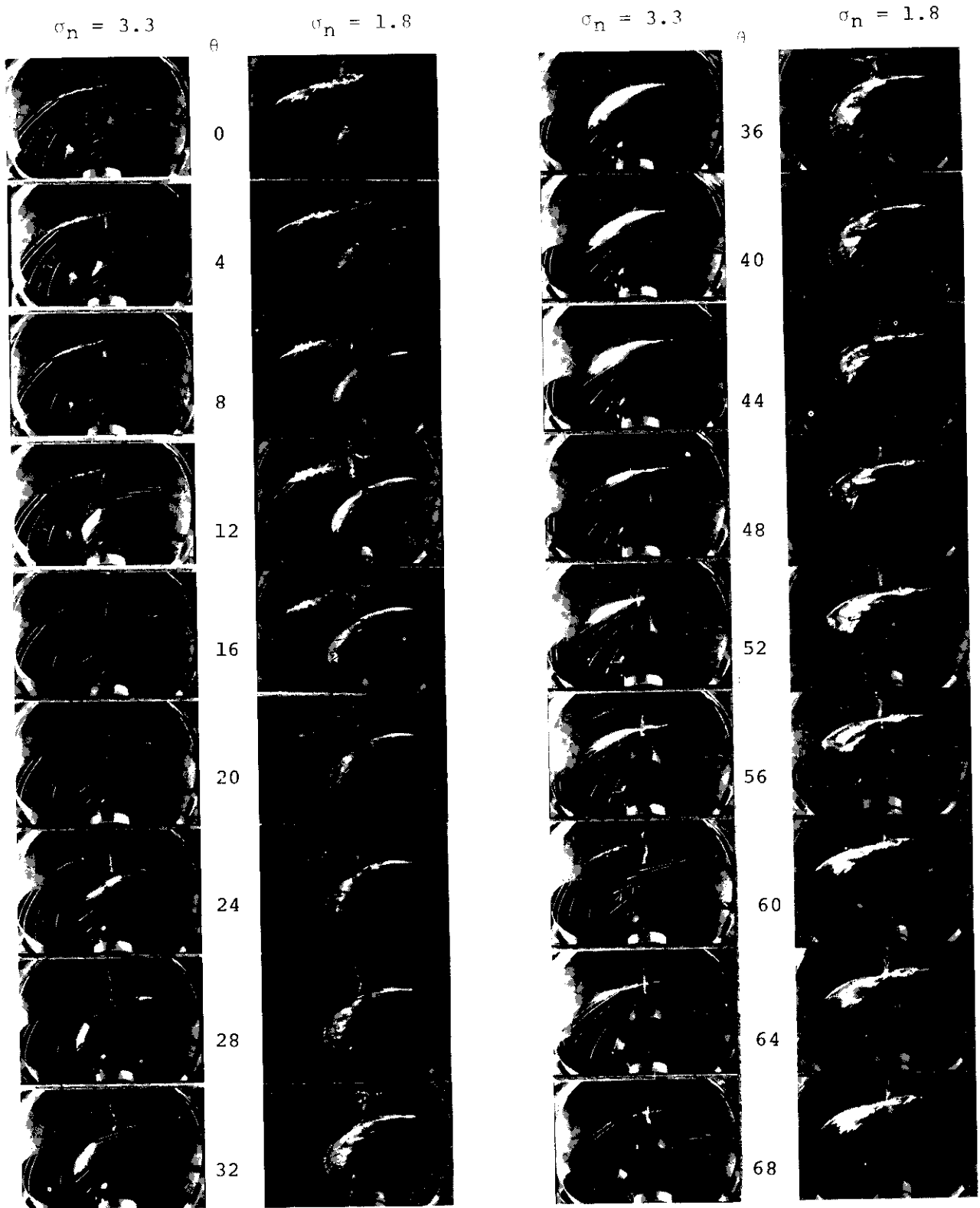


Fig. 23 Propeller 36W Pictured at Intervals of 4° and at Two Values of σ_n

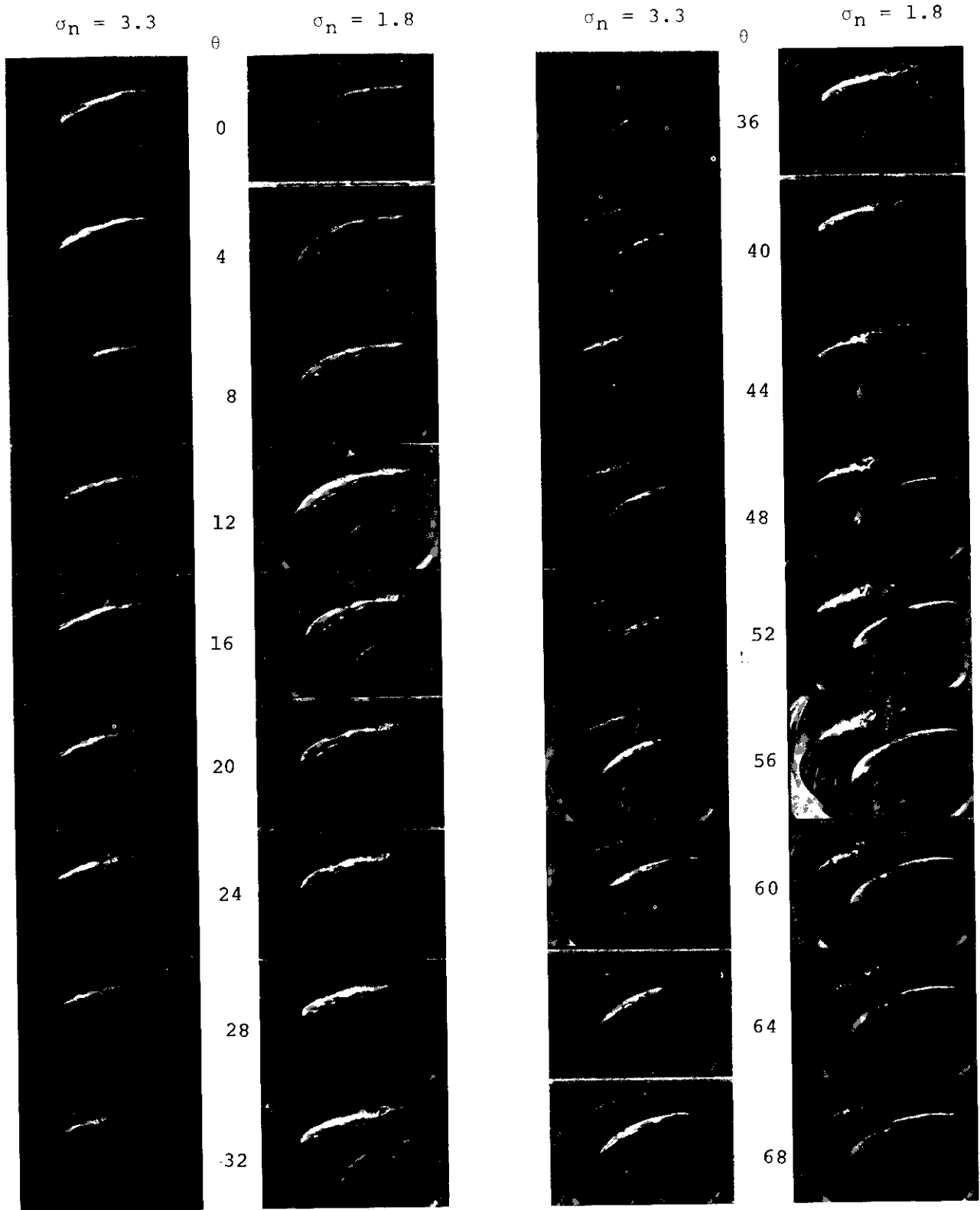


Fig. 24 Propeller 72W Pictured at Intervals of 4° and at Two Values of σ_n

imum extent of blade cavitation as a function of cavitation number, as well as the nature of the cavity collapse.

For the zero degree skew propeller, Figure 20, it is evident that at $\sigma_n=3.3$ the cavity collapses by moving out toward the tip, while for $\sigma_n=1.8$ the cavity initially rolls back from the leading edge.

The maximum extent of cavitation appears to decrease with increasing skew or warp, which one might anticipate on the basis of the relative intensity of the measured vibratory forces. There also appears to be more of a tendency for the cavity to collapse into the vortex as skew is increased.

In figures 20 and 21 for example, the photographic data for propellers 0S and 36S respectively are presented. Each column of photos is for a constant cavitation number, and propeller angular position advances in four degree increments from top to bottom of the page, continuing onto a second column.

Similarly, figures 22, 23, and 24 present results for propellers 72S, 36W and 72W respectively.

4. CONCLUSIONS

It was shown by the experiments done with a relatively simple arrangement that the transient cavitation has a significant role in propeller vibratory force. As transient cavitation becomes worse, the vibratory force is magnified by a factor of the order of 10 or more. This trend agrees with the results of previous research (1).

It was shown that skew and warp are effective in reducing vibratory force in both non-cavitating and cavitating cases. However, the relative magnitude of vibratory force with cavitation to that without cavitation is much higher for the skewed or warped propeller. In other words, we can say, skewed or warped propellers are sensitive to the influence of cavitation (Figures 10-12).

The higher harmonics, namely second and third, were not as large as we had expected. One possible reason for this is that these harmonics have a phase shift and the signals cancel each other on the force measuring disc. This is not the case for the first harmonic, on the other hand. The different sources which were implied from observing Figures 13-15 may underline it. Further investigation would be required to substantiate this.

The ratio of disc to propeller diameter was chosen so as to make these test results as realistic as possible. Therefore, it is felt that the relative change in hull vibration excitation for these propeller geometries should be applicable to the full-scale ship.

REFERENCES

1. E. Huse, "Cavitation-Induced Hull Pressures, Some Recent Developments of Model Testing Techniques," Symposium on "High Powered Propulsion of Large-Scale Ships," December 1974, Wageningen.
2. C. A. Johnsson, O. Rutgersson, S. Olsson and O. Björheden, "Vibration Excitation Forces From a Cavitating Propeller. Model and Full-Scale Tests on a High-Speed Container Ship," Eleventh Symposium on Naval Hydrodynamics, March 1976, London.
3. T. Sjøntvedt and H. Frivold, "Low-Frequency Variation of the Surface Shape of Tip Region Cavitation on Marine Propeller Blades and Corresponding Disturbances on Nearby Solid Boundaries," Eleventh Symposium on Naval Hydrodynamics, March 1976, London.
4. F. M. Lewis and J. E. Kerwin, "Vibratory Forces on a Simulated Hull Surface Produced by Transient Propeller Cavitation," prepared for SANME Panel H-8, February 1976.
5. R. J. Boswell, "Design, Cavitation Performance, and Open-Water Performance of a Series of Research Skewed Propellers," NSRDC Report 3339, March 1971.
6. R. A. Cumming, W. B. Morgan and R. J. Boswell, "Highly Skewed Propellers," SNAME Annual Meeting, November 1972, New York.
7. J. J. Nelka, "Experimental Evaluation of a series of Skewed Propellers with Forward Rake: Open-Water Performance, Cavitation Performance, Field-Point Pressures and Unsteady Propeller Loading," NSRDC Report 4113, July 1974.
8. J. K. Vandiver and C. A. Wales, "High-Speed Photography of Transient Cavitation on Marine Propellers," *High Speed Photography: Proceedings of the 12th International Congress on High Speed Photography*, August 1976, pp. 172-174, Toronto.
9. J. P. Breslin, "A Theory for the Vibratory Forces on a Flat Plate Arising from Intermittent Propeller Blade Cavitation," Symposium on "Hydrodynamics of Ship and Off-Shore Propulsion Systems," March 1977, Oslo.
10. E. Huse, "Effect of Tunnel Walls Upon Propeller-Induced Pressure in Cavitation Tunnels," Report of the Ship Research Institute of Norway, September 1973.

11. C. J. Gedney, "An Investigation of the Acoustical Characteristics of the M.I.T. Water Tunnel," M.I.T., Department of Ocean Engineering, Report 84188-1, January 1978.